Simulating Tethered Polymer Layers in Shear Flow with the Dissipative Particle Dynamics Technique

C. M. Wijmans and B. Smit*

Department of Chemical Engineering, University of Amsterdam, Nieuwe Achtergracht 166, 1018 WV Amsterdam, The Netherlands

Received January 17, 2002; Revised Manuscript Received June 10, 2002

ABSTRACT: The dissipative particle dynamics (DPD) method is used to simulate shear flow between two flat plates. To test this technique, simulations were conducted of both constant and oscillatory shear of a simple fluid. The results of these simulations agree well with theoretical predictions. We subsequently applied our model to study the effect of shear flow on end-tethered polymer layers ("brushes"). When exposed to a constant shear flow, chains in a polymer brush are stretched in the direction of the flow, and the overall layer thickness decreases. This result is similar to what was found in previous simulation studies. However, in the present simulations solvent particles are taken into account explicitly. At low frequencies, the response of a brush to oscillatory shear is qualitatively similar to its response to constant shear. As the flow velocity changes during an oscillation cycle, the polymer chains are able to relax their configurations with respect to the shear rate. At higher frequencies the interpretation of the brush behavior becomes more difficult due to conflicting time scales of the polymer and solvent dynamics in the present DPD model.

1. Introduction

Interactions between surfaces can be modified by adsorbing or grafting polymers to these surfaces. The fact that the polymers change not only the equilibrium properties but also the rheological properties is used in many applications. In simulations it is often much more difficult to study the dynamics of a system than its equilibrium state, and the simulation of solvent flow past and through a polymer layer forms a challenging problem. In this paper we apply the dissipative particle dynamics (DPD) method to study such a system. We will explore the possibilities of this technique by simulating various forms of shear flow for a simple fluid and study in detail grafted polymer layers under shear.

Over the past few years many papers have been published on end-tethered polymer layers. Much attention has especially been paid to so-called polymer brushes, high-density end-tethered layers, in which the polymer chains are strongly stretched away from the interface. Thanks to these investigations, the equilibrium behavior of such systems is now well understood.[1−10] However, nonequilibrium aspects of polymer brushes are, in general, less well understood. In this paper, we will focus on the effect that solvent flow past a polymer brush has on the properties of this brush.[11] As yet, no fully satisfactory answer to the question what happens to a polymer brush under shear seems to have emerged from the literature.

Two different kinds of experiments have been performed to investigate the effect of shear on a polymer brush immersed in a solvent. Klein et al.[12] designed a modified surface forces apparatus to measure the force between polymer-bearing surfaces undergoing shear. Their system consisted of two mica sheets bearing end-grafted polystyrene chains (which were tethered to the surface via a zwitterion group) in toluene (which is a good solvent for polystyrene). They found that as the surfaces were moved parallel to each other at a given frequency, a marked change occurred in the normal force between them. This force became increasingly repulsive as the velocity was increased. This effect was only seen above a certain critical shear rate, which was thought to be related to the relaxation dynamics of the polymer chains. The authors concluded that an uncompressed end-tethered polymer layer increases its thickness when fluid flows past it.

This conclusion is contradicted by experiments of polymer brushes under steady laminar shear flow. First, Nguyen et al.[13] used neutron reflectometry to measure polystyrene brushes. They reported no change in the brush height when solvent flowed past the brush, but this can be explained by the relatively low shear rate in their experiments. More convincing results were obtained by Baker et al.,[14] who constructed a cell in which fluid was pumped past an adsorbed polymer layer, giving plane Poisseuille flow. The system they used consisted of polystyrene−poly(ethylene oxide) diblock copolymer adsorbed onto a quartz surface from toluene. As the solvent flow velocity was increased, no changes occurred in the neutron reflectivity profile of the brush. The polymer volume fraction profile of the sheared brush was found to remain identical to that of the equilibrium brush up to shear rates at which substantial desorption of the polymer chains was observed. No extension of the tethered chains was found in these steady shear experiments. In addition, Ivkov et al.[15] published the results of neutron and reflectivity studies of polystyrene chains that were chemically end-tethered to a silicon oxide surface. They observed no change in the polymer brush profile or height even at the highest flow rates that were applied. A more extensive overview of the literature than we provide here can be found in the paper by Ivkov et al.[15]

On the theoretical side, several publications exist that consider the effect of shear on the layer thickness of a polymer brush, but here conclusions are not all in agreement with each other either. Several authors have derived analytic predictions for the effect of shear flow on grafted polymer layers.[16−20] The first models[16−18] ignored the details of solvent flow inside the brush by

10.1021/ma020086b CCC: $22.00
Published on Web 08/03/2002

assuming that the effect of the shear flow can be described by a shear force applied to the free surface of the brush. For example, the calculations of Rabin and Alexander[16] predicted no appreciable change of the brush layer thickness, whereas a similar model of Barrat[17] predicted brush swelling of up to 25%. This qualitative difference arises from a different contribution of the osmotic compressibility to the force acting at the free surface. Kumaran[18] calculated an even larger increase in the brush height from hydrodynamic interactions. Harden and Cates[19] took explicit account of both the solvent flow profile within a brush and the deformation of the grafted polymer chains within the Alexander−de Gennes brush model. In their calculations the internal structure of the layer and the solvent flow profile are determined self-consistently. They predicted nonuniform deformation of the grafted polymer chains and appreciable swelling (up to 25%) for shear rates exceeding the characteristic hydrodynamic relaxation rate of a blob of the unperturbed brush. This maximum swelling is even larger in the model developed by Aubuoy et al.,[20] in which some chains are stretched, whereas others remain unaffected by the shear. On the other hand, in a very recent theoretical analysis by Clement et al.,[21] it was predicted that the response of a brush to flow is typically of the same magnitude as thermal fluctuations.

The (strong) swelling of a polymer brush that is predicted theoretically is not seen in most molecular simulations of brushes that are sheared. Several simulation techniques have been used, such as Brownian dynamics,[22−24] stochastic dynamics,[25] and dynamic Monte Carlo.[26−28] One would expect the most exact results from molecular dynamics simulations, and such simulations have indeed been carried out for symmetric systems consisting of two layers of short grafted polymer chains which are sheared against each other.[29,30] However, most simulations of flow past polymer brushes tend to leave out the solvent molecules and model the solvent as a continuum to save CPU time. The Brinkman equation is then used to calculate the solvent flow through the polymer layer. This is the preferred method in Brownian dynamics simulations, where the solvent velocity and polymer concentration profile are calculated self-consistently. Although different authors use different models and also slightly different implementations of the Brownian dynamics algorithm, as a general trend it is found that under steady flow the brush thickness decreases as the shear rate increases.[22−24] However, Parnas and Cohen[22] report a maximum in the brush height as a function of shear rate for long chain lengths. Furthermore, Doyle et al.[23] report that oscillatory shear flow through a compressed brush leads to large increases in the normal stress. They interpret this result as a (qualitative) confirmation of the experimental measurements of Klein et al. However, simulated uncompressed brushes show only a relatively modest thickening under shear, and the diffuse tail region of the brush remains virtually unchanged. Finally, dynamic Monte Carlo simulations have been conducted of brushes under shear by introducing an enhanced transition probability for a monomer to move in the direction of the solvent flow.[26−28] In these cases very little effect of the shear was found on the overall polymer density profile perpendicular to the grafting surface. Of course, in these simulations hydrodynamic interactions are accounted for in a very approximate manner, as is also the case in the Brownian dynamics simulations.

In this paper we use the dissipative particle dynamics (DPD) method to simulate tethered polymer layers in shear flow. DPD is a particle-based simulation scheme that predicts correct hydrodynamic behavior (the overall movement of the particles obeys the Navier−Stokes equation). DPD particles do not represent individual atoms or solvent molecules, but fluid elements or parts of large molecules. Hoogerbrugge and Koelman[31,32] introduced the simulation method to study colloidal suspensions. Later on, it was, among other things, applied to study systems containing polymers, surfactant, and lipids.[33−39] Malfreyt and Tildesley[40] used the DPD technique to simulate equilibrium properties of polymer brushes. Español and Warren[41] showed that the DPD model corresponds to a Hamiltonian system. This created the possibility to conduct coarse-grained simulations of large equilibrium systems which are very hard to simulate using conventional microscopic simulation methods, such as surfactant phase diagrams,[37] lipid membranes,[36] and polymer−surfactant interactions.[39] In certain cases the hydrodynamic interactions are found to play a critical role in the attainment of equilibrium. Groot et al.[35] showed that this can be the case for block copolymer microphase separation, where simulation methods that neglect the hydrodynamics predict only metastable states.

The DPD method (applied to shear flow in confined geometries) is described in section 2. In section 3 we present results for the shear flow of a simple fluid (without polymer). This sets the scene for the simulation results of the grafted polymer layers. In section 4 we subsequently investigate hydrodynamic flow past a layer of tethered polymer chains.

2. Simulation Method

2.1. The Basic DPD Scheme. DPD is a Langevin dynamics scheme, in which one has a fluid of particles interacting through pairwise-additive interactions. These interactions consist of conservative forces, which determine the equilibrium behavior of the system, together with random and dissipative forces. We consider a system of volume $V = L_x \times L_y \times L_z$ with N particles i, each of which has a mass m, a position vector $\mathbf{r}_i$, and velocity $\mathbf{v}_i$. We define the number density as $\rho = N/V$. The particles obey Newton's equations of motion. The force on a particle i is

$$\mathbf{f}_i = \sum_{j \neq i} (\mathbf{F}_{ij}^{C} + \mathbf{F}_{ij}^{R} + \mathbf{F}_{ij}^{D}) \tag{1}$$

The conservative force $\mathbf{F}^C$ is a soft−repulsive interaction which is linear up to a cutoff distance r_c:

$$\mathbf{F}_{ij}^{C} = \begin{cases} a_{ij}(1 - r_{ij}/r_c)\hat{\mathbf{r}} & (r_{ij} < r_c) \\ 0 & (r_{ij} > r_c) \end{cases} \tag{2}$$

where a_{ij} is the repulsion parameter for an $i-j$ type interaction, $\mathbf{r}_{ij} = \mathbf{r}_i - \mathbf{r}_j$, $r_{ij} = |\mathbf{r}_{ij}|$, and $\hat{\mathbf{r}} = \mathbf{r}_{ij}/r_{ij}$. The random and dissipative forces, $\mathbf{F}^R$ and $\mathbf{F}^D$, are given by the following equations:

$$\mathbf{F}_{ij}^{R} = \sigma \omega^{R}(r_{ij}) \frac{\theta_{ij}}{\sqrt{\Delta t}} \hat{\mathbf{r}}_{ij} \tag{3}$$

$$\mathbf{F}_{ij}^{D} = -\gamma \omega^{D}(r_{ij})(\hat{\mathbf{r}}_{ij} \cdot \mathbf{v}_{ij})\hat{\mathbf{r}}_{ij} \tag{4}$$

where $\mathbf{v}_{ij} = \mathbf{v}_i - \mathbf{v}_j$, σ is the noise amplitude, γ is the friction coefficient, $\omega^R(r_{ij})$ and $\omega^D(r_{ij})$ are weight functions which become zero for $r \geq r_c$, and θ_{ij} is a random Gaussian variable with zero mean and a variance of unity. Espanol and Warren[41] showed that the condition of detailed balance imposes the following constraints on the weight functions and constants:

$$(\omega^R(r_{ij}))^2 = \omega^D(r_{ij}) \tag{5}$$

$$\sigma^2 = 2k_B T\gamma \tag{6}$$

We take

$$\omega^D(r_{ij}) = \begin{cases} \left(1 - \frac{r_{ij}}{r_c}\right)^2 & (r_{ij} < r_c) \\ 0 & (r_{ij} \geq r_c) \end{cases} \tag{7}$$

and we set $\sigma = 3.0$. It is furthermore convenient to work with simulation units $m = k_B T = r_c = 1$.

The simulation method as described thus far is the standard DPD scheme. The positions and velocities of the particles are calculated using a modified Verlet algorithm.[34] All simulations were conducted with a time step $\Delta t = 0.01$.

2.2. Tethered Polymer Chains. In our simulation model a polymer chain is represented as a linear array of M particles. The total number of particles in the system is $N = N_s + N_p M$, with N_s the number of solvent particles and N_p the number of polymer chains. In addition to the repulsive conservative force and the random and dissipative forces, bead $i + 1$ exerts a bonding force $\mathbf{F}^b_{i,i+1}$ on bead i, which is given by

$$\mathbf{F}^b_{i,i+1} = \begin{cases} -10 \times \mathbf{r}_{i,i+1} & \text{for } r_{i,i+1} < r_c \\ -110 \times \mathbf{r}_{i,i+1} & \text{for } r_{i,i+1} > r_c \end{cases} \tag{8}$$

The precise form of the bonding interaction that we have used is rather arbitrary and will be justified a posteriori. The polymer chains are attached to an impenetrable surface at $z = 0$. The same attractive force that exists between neighboring segments also exists between the first segment in each polymer chain and a "tethering position" on the surface. These tethering points form a regular square grid. At the other end of the simulation box ($z = L_z$) we place a similar surface without any polymer.

2.3. Shear Flow. In molecular dynamics, the standard way to model shear flow is by applying the Lees−Edwards boundary condition.[42] In DPD one can actually shear a liquid by moving a solid wall past the liquid. In our simulations, the upper surface is given a velocity in the y-direction $v_y(L_z) = v^*$ and the lower surface is given a velocity $v_y(0) = 0$. Modeling a liquid−solid interface in DPD is, however, not a completely trivial task, and one must be aware not to introduce unwanted artifacts into the simulation.

Kong et al.[33] studied the dynamics of a DPD polymer in solution between two walls (without shear). Wall particles were kept in a "frozen" state, so that they could not move relative to each other. (This is an analogous procedure to that used to model dispersions.) The density of the wall had to be chosen 4 times larger than that of the solution to get an impenetrable wall. This high density subsequently induces a depletion zone in the solution adjacent to the wall. Although such a depletion layer and further ordering phenomena are to be expected at the atomistic level, they must be seen as model artifacts in a coarse-grained model. A similar nondesired effect of the model is seen in the simulation of Jones et al.,[43] who simulated the shearing of a liquid drop on a solid surface. They used the same density for the solid and liquid but added a strong repulsive interaction between both phases to keep them separated. Again, this leads to density distortions in the liquid. Moreover, the flow profile shows the occurrence of large slip. Jones et al. attempted to solve this problem by imposing a certain velocity on all particles within a close distance from the wall. Revenga et al.[44] suggested that slip can be prevented by using a large ratio (of nine) for the densities of the wall and solution. In their work no repulsive interactions between particles are taken into account, and in this case such a high ratio does indeed solve the problem of slip. However, in general, ideal particles will not be a good model for a molecular system. When interactions between particles are added, such a high-density ratio leads to very large density distortions in the solution.

The problems mentioned above concerning density distortions and slip flow only play a role near the surface. If one is solely interested in the behavior of the sytem far away from any interfaces, these issues do not pose a problem. However, in many applications one is dealing with systems where the effect of surfaces cannot be neglected, for example, in lubrication. In such confined geometries the conventional DPD method will easily give rise to unwanted artifacts. Recently, Willemsen et al.[45] proposed a scheme to get a no-slip boundary condition in DPD without using high wall densities, which we have applied in our simulations. Below we give a brief description of this algorithm. More details can be found in ref 45.

The walls are assumed to be made up of "virtual" particles. The interactions between the real fluid particles (which can be both solvent particles or polymer segments) and these wall particles are determined by the same equations that describe the forces between two fluid particles. However, the positions and velocities of the wall particles are not updated using the Verlet or a similar algorithm. At the beginning of each time step they are determined in such a way as to ensure a smooth distribution of fluid particles near the walls together with no-slip conditions. For each fluid particle whose distance to the wall is smaller than r_c, a wall particle is placed at the same distance from the boundary layer. The x and y components of the wall particle are determined by adding a random shift taken from the interval $(-r_c, r_c)$ to the position of the original fluid particle. The normal (z) and the x velocity components of the wall particle have the same magnitude as those of the original fluid particle, but the sign of these components is opposite to that of the fluid particle. The y velocity component of the wall particle is taken as the average of the y velocity component of the fluid particle and the wall velocity. This procedure ensures that there is a linear velocity profile across the wall boundary. The random and drag forces exerted by the wall on nearby fluid particles (those at a distance smaller than r_c) are calculated by summing over all pair interactions between fluid and wall particles. However, the conservative forces are calculated from a different set of wall particle positions, as the interactions between the fluid particles directly adjacent to the wall and their own mirror images lead to a too large repulsion. Therefore,

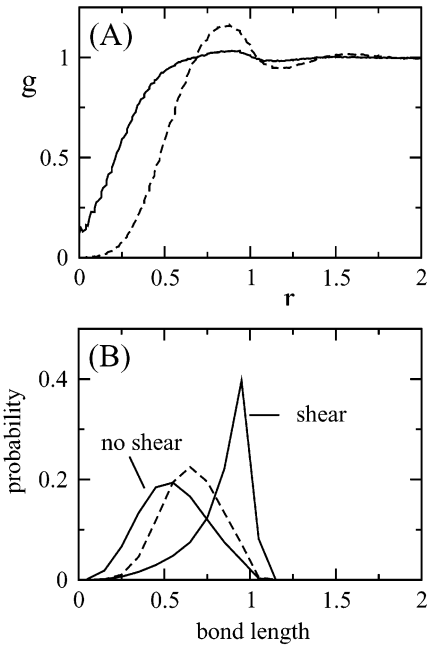

Figure 1. Solvent radial distribution functions (A) and polymer bond length distributions (B). In (A) the full curve shows $g(r)$ for $\rho = 10$ and $a = 10$ (parameter set 1), and the dashed curve shows $g(r)$ for $\rho = 3$ and $a = 25$ (parameter set 2). In (B) the polymer bond length distributions are shown for the same two systems. For $\rho = 10$ the distribution is shown for polymer chains in an unsheared brush and for a single chain in a solvent flow field. For $\rho = 3$ the distribution is only shown in the absence of shear (dashed curve).

a second set of wall particles is created by shifting all fluid particles at a distance between r_c and $2r_c$ into the wall layer. These wall particles are then used to calculate the conservative force exerted by the wall on the fluid.

A straightforward extension of the above algorithm also makes it possible to simulate shear flow in a curved (cylindrical) geometry.[46]

2.4. Parameters. As standard parameters, we choose a box size $L_x \times L_y \times L_z = 8 \times 8 \times L_z$, a particle density $\rho = 10$, polymer chain length $M = 20$, and repulsion parameter $a = 10$. We denote these values as "parameter set 1". The (relatively high) value for the particle density ensures that the no-slip boundary condition is well obeyed at the upper wall without any large density distortions due to the surface interactions.[45] The number of tethered polymer chains ranges from $N_p = 1$ to 100. The lower surface is always kept at rest, whereas the upper surface is given a velocity v^*, determining the shear rate $\dot{\gamma} = dv_y/dz$. In addition, we consider an alternative system with a fluid density $\rho = 3$ and repulsion parameter $a = 25$. We refer to these values as "parameter set 2". This lower density can be simulated more quickly, so that we consider longer polymer chains with $M = 60$. Groot and Warren[34] devised a mapping procedure to link DPD parameters to molecular systems using these values for ρ and a. Several authors have since used this combination of parameters to model aqueous polymer and surfactant systems.[34,36,38,39]

Figure 1a shows the radial distribution function $g(r)$ of an isotropic DPD fluid with $\rho = 10$ and $a = 10$ (parameter set 1) together with the same curve for $\rho = 3$ and $a = 25$ (parameter set 2). Note that for $\rho = 10$ this function remains finite as the distance r goes to zero. Furthermore, the distribution function has few distinctive features, showing only one, very weak, maximum at $r \approx 0.7-0.8$. For a particle density $\rho = 3$ one finds a radial distribution function which becomes zero at small distances and which has a far more pronounced maximum (for $r < 1$) together with less pronounced maxima for $r > 1$.[34,53] The distribution function for $\rho = 10$ is characteristic of a more strongly coarse-grained system, where a DPD particle represents a larger number of solvent molecules (or polymer segments). The precise form of the bond force between neigboring polymer segments given by eq 8 is relative arbitrary, and different expressions can be found for this interaction in the literature.[34,38,40] For polymers in equilibrium, eq 8 gives an approximately symmetric bond length distribution with a maximum at approximately $0.55r_c$. This is illustrated for a polymer chain in an unsheared brush in Figure 1b. The same graph also gives the distribution for a (very) strongly sheared chain. In this case this distribution is highly asymmetric, the maximum occurring for a bond length slightly lower than r_c. Few bond lengths exceed r_c because of the strongly increasing attractive force for bonds that stretch beyond this distance.

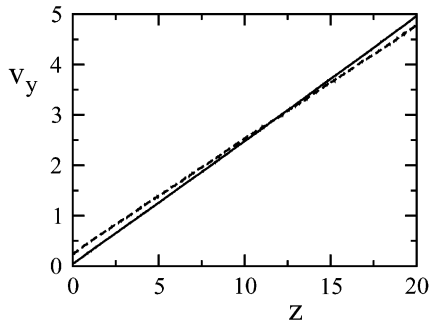

Figure 2. Steady-state velocity profiles for two different densities: $\rho = 3.0$ (dashed line, (parameter set 1)) and $\rho = 10$ (full line, (parameter set 2)). Further parameters: $L_x = L_y = 8$, $L_z = 20$, $v_y(0) = 0$; $v^* = 5.0$; $a = 10$ for $\rho = 10$ and $a = 25$ for $\rho = 3$.

3. Results and Discussion

3.1. Simple Fluids. In this section we consider the shear behavior of a one-component fluid. Although in itself this is not an extremely interesting or challenging system to simulate, it does provide a benchmark to explore the possibilities and limitations of the DPD method to model shear. In the next section we will move on to the more complex system of a polymer brush in a shear flow.

3.1.1. Constant Shear. Figure 2 shows results for the steady-state flow profile using the algorithm described in the previous section for two different densities. The lower density of $\rho = 3.0$ clearly leads to slip flow at both surfaces. However, the velocity profile does remain a linear function right up to the surface. The higher density of $\rho = 10.0$ gives rise to virtually no slip. In this case the shear velocity approaches its ideal value $dv_y/dz = v^*/L_z$. We found this trend of increasing slip with decreasing density for a wide range of parameter values. The repulsion parameter a has little effect on the occurrence of slip. The qualitative trends are furthermore similar for a wide range of shear velocity values. Correlations between the z and y components of the (average) particle velocities cause the slip. We conclude that the DPD shear algorithm works well for high particle densities ($\rho \geq 10$). For low densities one

still clearly gets slip. However, in (many) applications this will not be of great consequence unless one is specifically interested in the properties of the actual wall−fluid interface.

The velocity profile of a simple fluid between two walls as we have simulated can also be calculated analytically. We have to solve the following differential equation for $v = v_y(z,t)$:

$$\frac{\partial v}{\partial t} = \nu \frac{\partial^2 v}{\partial z^2} \tag{9}$$

where $\nu = \mu/\rho$ is the kinematic viscosity of the liquid (μ is the dynamic viscosity). The reduced units of ν are $r_c(kT/m)^{1/2}$. If we solve eq 9 with the following boundary conditions

$$\begin{aligned} v_y(0, t) &= 0 \\ v_y(L_z,t) &= v_y(L_z) = v^* \\ v_y(z,0) &= 0 \end{aligned} \tag{10}$$

we find that[47,51]

$$v_y(z,t) = v_y(L_z)\sum_{n=0}^{\infty}\left(\operatorname{erfc}\left(\frac{(2n+1)L_z - y}{2\sqrt{(\nu t)}}\right) - \operatorname{erfc}\left(\frac{2nL_z + y}{2\sqrt{(\nu t)}}\right)\right) \tag{11}$$

For long times eq 11 reduces to the steady-state solution

$$v_y(z) = \frac{v^* z}{L_z} \tag{12}$$

and for short times only the first term on the right-hand side for $n = 0$ is significant, which reduces eq 11 to

$$v_y(z,t) = v^* \operatorname{erfc}\left(\frac{L_z - z}{2\sqrt{\nu t}}\right) \tag{13}$$

Willemsen et al.[45] showed that fitting eq 13 is a computationally efficient alternative to simulating the stress tensor to find the viscosity of a system. Using this method, we find a value of $\nu = 0.25$ for a system with $a = 10$ and $\rho = 10$. The viscosity is practically constant as a function of the repulsion parameter a. The viscosity does depend on ρ and T, so this offers some scope to fit an experimental system with a simulation model. As a first-order approximation, one can use the prediction of Marsh et al.[48] that $\nu \sim \rho/k_BT$, although numerical calculations show small deviations from this theory.[45,49,50]

3.1.2. Oscillatory Shear. We now investigate a fluid in an oscillatory shear field. The lower wall is again kept at zero velocity. The upper wall is given a sinusoidal displacement $\Delta(t)$

$$\Delta(t) = \frac{V_{max}}{\omega}(\cos(\omega t) - 1) \tag{14}$$

so that

$$v^* = v_y(z=L_z,t) = V_{max} \sin(\omega t) \tag{15}$$

The expected fluid flow response $v_y(z,t)$ of a fluid with viscosity ν can again be derived analytically.[51,52] The flow profile consists of a transient and a steady-state term:

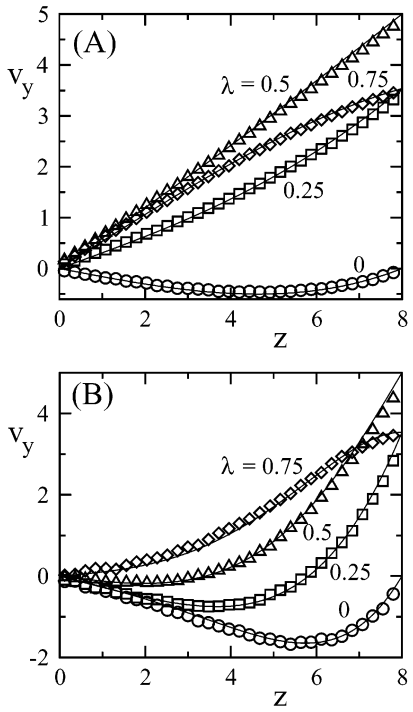

Figure 3. Velocity profiles for oscillatory flow: $v_y(z)$ for $t = \lambda(\pi/\omega)$ (mod 2π) with $\lambda = 0$, 0.25, 0.5, and 0.75. The simulated profiles are compared with the prediction of eq 17 for $\nu = 0.25$. Parameters: $f = 0.001$ (A) and $f = 0.01$ (B); $v_y(0) = 0$, $V_{max} = 5.0$; $L_x = L_y = L_z = 8$; $a = 10$; $\rho = 10$.

$$v_y(z,t) = T(z,t) + S(z,t) \tag{16}$$

where the transient term $T(z,t)$ becomes zero at large t.[51,52] The oscillatory steady-state term $S(z,t)$ can be written as

$$S(z,t) = AV_{max} \sin(\omega t + \phi) \tag{17}$$

with

$$A = \left(\frac{\cosh(2(\omega/2\nu)^{1/2}z) - \cos(2(\omega/2\nu)^{1/2}z)}{\cosh(2(\omega/2\nu)^{1/2}L_z) - \cos(2(\omega/2\nu)^{1/2}L_z)}\right)^{1/2} \tag{18}$$

and

$$\phi = \arg\left(\frac{\sinh((\omega/2\nu)^{1/2}z(1+i))}{\sinh((\omega/2\nu)^{1/2}L_z(1+i))}\right) \tag{19}$$

We are mainly interested in the oscillatory steady-state solution rather than the transient term. Figure 3 shows simulated velocity profiles from a production run of eight cycles after two equilibration cycles for a frequency $f = \omega/2\pi$ of 0.001 and 0.01, using similar parameters as in the previous section ($L_x = L_y = L_z = 8.0$; $a = 10.0$; $\rho = 10.0$). When fitting the analytical expression, we again used $\nu = 0.25$. Rather than plotting the flow velocity (for different z) as a function of time, Figure 3 shows $v_y(z)$ for $t = \lambda(\pi/\omega)$ (mod 2π) for various values of λ (Of course, $v_y(z,\lambda(\omega/\pi)) = -v_y(z, (\lambda + 1)(\omega/\pi))$). In Figure 3 comparisons are made between the simulations and the analytical expressions for $\lambda = 0$, 0.25, 0.5, and 0.75. The simulated profiles agree well with the analytical predictions. Slight deviations are

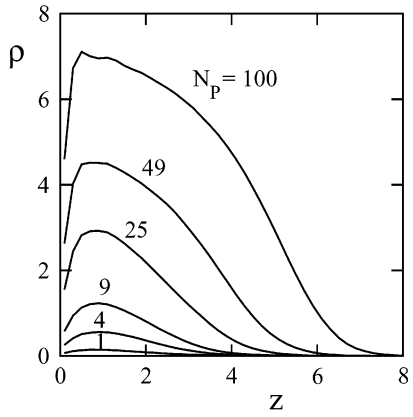

Figure 4. Density profiles of end-tethered polymer layers at equilibrium (i.e., in the absence of shear) for various grafting densities. Parameters: $N_p = 1$, 4, 9, 25, 49, and 100 (as indicated); $L_x = L_y = 8$; $M = 20$; $a = 10$; $\rho = 10$. For these five grafting densities the values of H_{rms} are 1.68, 1.71, 1.75, 1.98, 2.36, and 2.99, respectively.

found, especially at the surfaces, as the effect of slip has a greater effect due to the continual change of the wall velocity. However, this has only a very minor effect on the overall velocity profile.

3.2. Tethered Polymer Layers. In the previous section we have demonstrated the suitability of the DPD to simulate shear flow near a solid surface. We will now apply this method to study the response of end-tethered polymer layers to shear flow. Most of the results we report are obtained using parameter set 1. In addition, some results are reported using parameter set 2. We conclude this section with a short comparison of the results found for the two parameter sets.

3.2.1. Density and Flow Velocity Profiles (Parameter Set 1). Figure 4 shows simulated equilibrium density profiles (i.e., in the absence of shear flow) for a number of different grafting densities. The lowest density ($N_p = 1$) corresponds to the "mushroom" regime, where the tethered chain basically forms a random coil in the available half ($z > 0$) of the three-dimensional space. At the highest densities, we are dealing with strongly stretched chains forming a brush configuration with a parabolic density profile. Because of the relatively short chain length, the density profiles have a pronounced exponentially decaying "foot" at their outer edge. At the grafting surface the profiles show a distinctive dip due to entropic repulsion. Such a depletion zone is well-known from Monte Carlo simulations,[5] numerical SCF calculations,[8] and neutron scattering experiments.[7] No spurious oscillatory distortions occur in our simulated density profiles. For each system we define a root-mean-square (rms) layer thickness as

$$H_{rms} = \left(\frac{\int_0^{L_z} \rho_{pol}(z) z^2 \, dz}{\int_0^{L_z} \rho_{pol}(z) \, dz} \right)^{1/2} \qquad (20)$$

The values of H_{rms} for the profiles in Figure 4 are given in the caption of that figure. For $N_p \geq 49$ the relationship between the root-mean-square layer thickness and the grafting density (which is proportional to N_p) is in agreement with the scaling relationship $H_{rms} \sim N_p^{1/3}$, which is what one expects for a brush in a good solvent.

When the system is sheared by moving the upper surface, the solvent velocity profile can be determined. An example of the velocity profile is shown in Figure 5

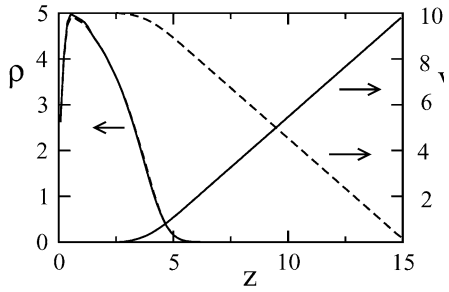

Figure 5. Density profiles and solvent velocity profiles of a sheared brush. The full curves refer to simulations where the system was sheared by moving the upper surface ($v^* = 10$), and the dashed curves are for simulations where the lower surface (with the polymer layer) was moved. The two density profiles overlap and can hardly be distinguished from each other. The number of polymer chains is $N_p = 49$, and all other parameters are the same as in Figure 4.

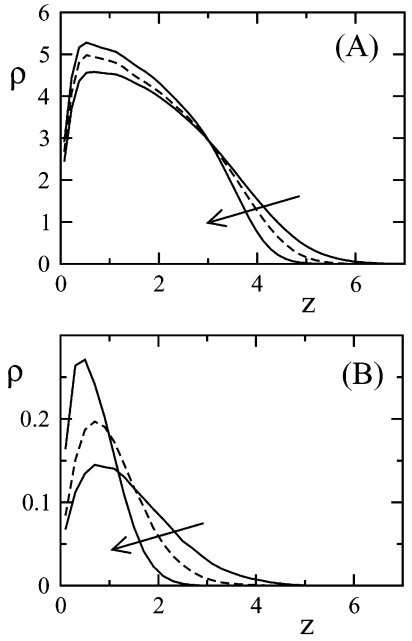

Figure 6. Density profiles of sheared and unsheared grafted polymer layers. In (A) a high grafting density is used, $N_p = 49$, and in (B) a low grafting density is used, $N_p = 1$. In both cases the grafting surface is $L_x \times L_y = 8 \times 8$. In (A) the shear rates are $\dot{\gamma} = 0$, 0.88, and 1.7, and in (B) $\dot{\gamma} = 0$, 0.10, and 0.50. The arrows indicate the direction in which the shear rate increases.

for a system with $N_p = 49$, which corresponds to the brush regime. In this example the velocity of the upper surface $v^* = 10$. The applied shear leads to a compression of the polymer layer in comparison with the equilibrium situation. The root-mean-square layer thickness of the sheared brush is 8% smaller than that of the unsheared brush. The shear rate $\dot{\gamma}$ is defined by the solvent profile above the polymer layer, which gives a value $\dot{\gamma} = 0.88$. Following Doyle et al.,[23] we use the Weissenberg number (Wi) to represent the shear rate as a dimensionless number which can be compared with experimental values. This dimensionless number is defined by Doyle et al. as the product of the relaxation time τ of a single chain in solution[38] and the shear rate $\dot{\gamma}$: $Wi = \tau\dot{\gamma}$. We calculated τ from the temporal decay of the polymer end-to-end vector. In our case, the value of the Weissenberg number is $Wi = 19$, which falls within the range of values considered by Doyle et al.[23] Doyle et al. chose their parameters to be in the same range

as those in the experiments of Klein et al.[12] By linearly extrapolating this profile to $v_y = 0$, we find the hydrodynamic thickness of the polymer layer, H_{hyd}. We also applied shear to this system by conducting the reverse simulation in which the lower surface with the polymer layer is moved and the velocity of the upper surface is kept zero. This gives the same shear rate and polymer layer thickness. The polymer density profiles in Figure 5 for the two simulation setups can hardly be distinguished from each other. Below, in all simulations the upper surface is moved and the lower, polymer-bearing surface is kept at rest.

In Figure 6 polymer density profiles are compared for different shear rates and different grafting densities. The grafting density in Figure 6A ($N_p = 49$) corresponds to a polymer brush, and that in Figure 6B ($N_p = 1$) corresponds to a "mushroom" structure. In both cases the layer thickness decreases as the shear rate increases. The shear rates that were applied in the brush simulations were $\dot{\gamma} = 0.88$ and 1.7. The root-mean-square layer thicknesses of these sheared brushes were 8% and 15% smaller than the thickness of the unsheared brush. The low-density grafted layer was subjected to lower shear rates of $\dot{\gamma} = 0.10$ and 0.50. The value of H_{rms} decreased by 24% and 48%, respectively.

The qualitative picture that emerges from these simulations agrees well with that of the Brownian dynamics simulations of Doyle et al.[23] A constant shear compresses the grafted polymer layers, and for a given shear rate, the compression effect becomes smaller as the grafting density increases. This effect is most prominent for polymer chains that are tethered to the surface at such low densties that they form isolated coils. Although these "mushroom" conformations are less interesting from a theoretical point of view, they can be of great practical importance in many systems where the polymer density on the surface is too low to form brush structures.

The DPD simulations are not based on any assumptions concerning the form of the velocity profile in the polymer layer. These simulations can therefore be used to check the validity of theories that describe the solvent flow, such as the Brinkman equation for the velocity $v = v_y(z)$:

$$\frac{d^2v}{dz^2} = \frac{v}{k^2} \tag{21}$$

where the friction coefficient k is a function of the polymer concentration only: $k = k(\rho_{pol})$. The value of k is mostly set equal to the screening length ξ of a polymer solution at density ρ_{pol}. Assuming that eq 21 is correct, we have derived values for $k(\rho_{pol})$ from simulated flow profiles.[54] Figure 7 shows these functions for various systems (different polymer densities and shear rates). For each data set in this figure the values become unreliable at high ρ (i.e., deep within the polymer layer), where the solvent flow has become zero. The same is true for very low values of ρ, where the velocity profile is practically linear. However, we can identify an intermediate region (roughly for $0.1 < \rho < 1$) where the data from the different sets collapse nicely onto a master curve. Here we find the following relationship between the friction coefficient and the polymer density: $k \approx \rho^{-0.55}$. This exponent (which is indicated by the arrow in Figure 7) differs significantly (that is, more than can be explained by numerical inaccuracy in its derivation)

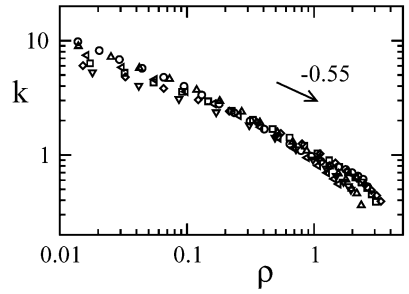

Figure 7. Friction coefficient k in the Brinkman equation as a function of the polymer density ρ. The arrow indicates a slope of -0.55. The symbols refer to simulations with different polymer densities and shear rates: (○) $N_p = 49$ and $\dot{\gamma} = 0.092$; (□) $N_p = 49$ and $\dot{\gamma} = 0.88$; (◇) $N_p = 49$ and $\dot{\gamma} = 1.7$; (△) $N_p = 25$ and $\dot{\gamma} = 0.29$; (tilted △) $N_p = 9$ and $\dot{\gamma} = 0.54$; (▽) $N_p = 9$ and $\dot{\gamma} = 1.1$. In all cases $M = 20$.

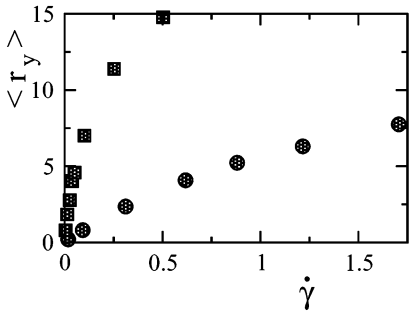

Figure 8. Average value of the y component of the end-to-end vector $\langle r_y \rangle$ of polymer chains in a tethered layer as a function of shear rate $\dot{\gamma}$: circles, $N_p = 49$; squares, $N_p = 1$.

from the relationship $\xi \sim \phi^{-3/4}$, which holds for a semidilute polymer solution and which was used in the brush simulations of refs 26 and 27.

3.2.2. Chain Tilting. Besides compressing the grafted layer, the solvent flow also causes the polymer chains to become oriented in the y direction. The average y component of the "end-to-end" vector connecting the surface tether with the last segment $\langle r_y \rangle$ is shown in Figure 8 as a function of the shear rate. For $\dot{\gamma} = 0$ we must necessarily have $\langle r_y \rangle = 0$, and all deviations from this value are due to statistical fluctuations. For low grafting densities, the polymer chains stretch more strongly in the flow direction with increasing shear rate. This is not surprising as the solvent flow penetrates further into a low-density grafted layer than into a high-density one. For the lowest grafting density, which corresponds to one polymer chain in the system, we find a value $\langle r_y \rangle = 15$ for $\dot{\gamma} = 0.5$. This is larger than the simulation box size, indicating that on average the chain wraps around the system nearly two times. At the same shear rate the value of $\langle r_y \rangle$ is more than 3 times smaller for the higher density layer with $N_p = 49$.

The data shown in Figure 8 are averages over all polymer chains in the grafted layer. However, a brush is made up of chains with different configurations. The distribution perpendicular to the surface of free end segments in a sheared brush (with the same parameters as used in Figure 5) is given by the dashed curve in Figure 9. This figure also shows the average y component of the end-to-end vector of a polymer chain whose end segment is located at a given distance z from the tethering surface. Polymer chains that stretch farthest away from the surface also become most strongly stretched in the flow direction. This can easily be understood, as the solvent flow is strongest at the

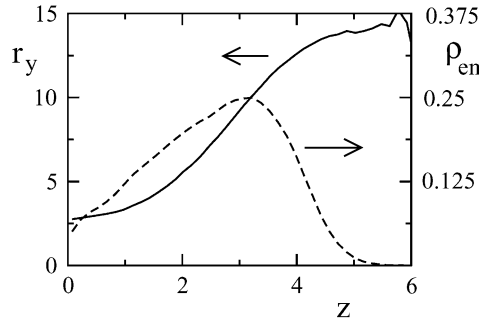

Figure 9. Distribution of free end segments in a sheared polymer brush (at a shear rate $\dot{\gamma} = 1.7$; this is exactly the same system as shown in Figure 5). The full curve shows the average value of the y component of the end-to-end vector $\langle r_y \rangle$ of a polymer chain whose end segment is located at a distance z from the tethering surface. The dashed curve gives the end segment density distribution $\rho_{end}(z)$ perpendicular to the surface.

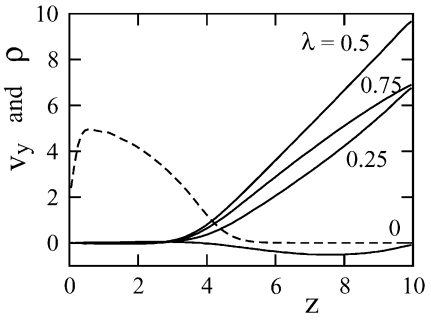

Figure 10. Velocity profiles for oscillatory flow in the presence of a polymer brush. The solvent flow velocity $v_y(z)$ is shown for $t = \lambda(\pi/\omega)$ (mod 2π) with $\lambda = 0$, 0.25, 0.5, and 0.75. These profiles can be compared with those in Figure 3A, where there is no polymer present. The dashed curve shows the (time-averaged) polymer density profile. Parameters: $f = 0.001$, $V_{max} = 10$, $L_x \times L_y \times L_z = 8 \times 8 \times 10$, $N_p = 49$.

outside of the brush. However, chains whose free segment is very near the tethering surface are, on average, still stretched to a significant extent in the flow direction. This is slightly unexpected as the solvent flow is zero so near the surface. The explanation for this phenomenon lies in the fact that even for these chains some segments along the chain can stick out farther away from the surface and thus experience the solvent flow. The chain length used in Figure 9 ($M = 20$) is relatively small, so that the mean-field description of a polymer brush, which excludes chains folding back to the tethering surface,[3,6] is not fully valid. For longer chain lengths we expect the curve in Figure 9 to decrease more rapidly to zero for small z.

3.2.3. Oscillatory Shear (Parameter Set 1). In addition to steady shear flow, we have also studied the response of grafted polymer layers to oscillatory shear flow. These simulations are especially relevant with regard to the interpretation of the experiments which show a swelling of polymer brushes under oscillatory shear. Rather than moving the upper surface at a constant velocity, its velocity becomes a sinusoidal function of time with amplitude V_{max}. Again, we focus on a brush with $N_p = 49$ in a simulation box of size $L_x \times L_y \times L_z = 8 \times 8 \times 10$. Velocity profiles for this system, similar to those in Figure 3, are shown in Figure 10 for $f = 0.001$. The dashed curve is the average polymer density profile. As the direction and magnitude of the solvent flow are not constant, the precise form of the density profile is also a function of time. The

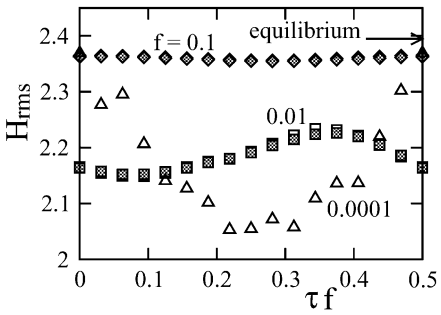

Figure 11. Root-mean-square layer thickness H_{rms} as a function of time during (half) an oscillation cycle for frequencies $f = 0.0001$ (triangles), 0.01 (squares), and 0.1 (diamonds). All parameters are the same as in the previous figure. The arrow indicates the layer thickness of an unsheared brush. The white and gray symbols for $f = 0.1$ and 0.01 refer to independent simulation runs. These can hardly be distinguished from each other. Resulst of one simulation run only are shown for $f = 0.0001$.

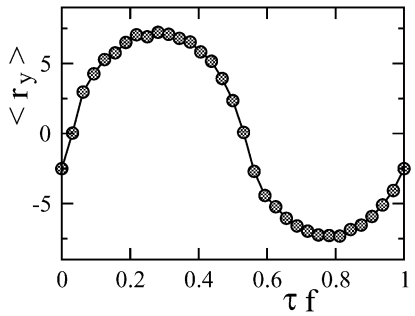

Figure 12. Average value of the end-to-end vector $\langle r_y \rangle$ during the oscillation cycle. All parameters are the same as in Figure 10 ($f = 0.001$).

penetration of the solvent flow into the grafted layer is similar to what we observed in the case of constant shear.

In Figure 11 the layer thickness is shown for three different oscillation frequencies in the range $f = 10^{-4}$–0.1. In reduced units τf these frequencies lie in the range 2×10^{-3}–2. The value of H_{rms} is shown as a function of time t during half on oscillation cycle (from $t = 0$ to $t = 0.5/f$). For two frequencies the results of two independent runs are shown, indicating the statistical error in these results, which is small for the highest two frequencies that are plotted. For $f < 0.01$ this statistical error is larger. The arrow in Figure 11 indicates the layer thickness of an unsheared brush. At low frequencies ($f \leq 0.001$) the layer is compressed, although the layer thickness is not constant throughout the oscillation cycle. The thickness oscillates around its average value of $H_{rms} = 2.16$. The continuous change in the thickness is due to the continuously varying shear rate experienced by the polymer brush. The response of the grafted layer to the change in shear rate is also reflected in the orientation of the polymer chains. Figure 12 shows the average value of the end-to-end vector $\langle r_y \rangle$ vs time during the oscillation cycle. The chain ends clearly move toward the $+y$ and $-y$ directions as the solvent flows in that direction. These results indicate that the polymer layer is able to relax with respect to the change in shear rate. At any point during the oscillation cycle the polymer chains respond more or less similarly to the oscillating shear flow as they would respond to a constant shear with the same instantaneous shear rate.

In Figure 11 one can further see that as the oscillation frequency increases, the amplitude of the function

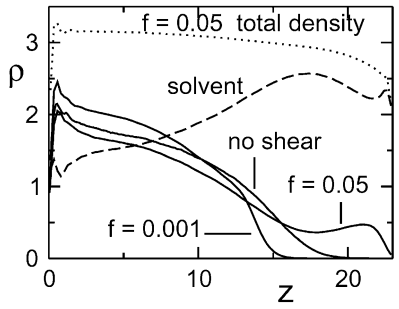

Figure 13. Density profiles of a polymer brush using parameter set 2. The upper wall performs an oscillatory motion with amplitude $V_{max} = 40$ and frequency $f = 0.001$ and 0.05. The profile of an unsheared brush is shown for comparison. For $f = 0.05$ the total density profile (the sum of the polymer and solvent profiles) is also shown. For $f = 0.001$ the total density profile is practically identical to that of the unsheared system.

$H_{rms}(t)$ becomes smaller, and the average value of H_{rms} increases. For $f = 0.1$ the layer thickness becomes equal to that of the equilibrium brush. This may indicate that at higher frequencies the brush cannot relax to its most preferred conformation during the oscillation cycle. However, there is one problem that interferes with a straightforward comparison of the simulations at different frequencies. The shear rates that are experienced by the brush are not the same for all frequencies. At higher frequencies the velocity profiles decay more quickly as one moves away from the oscillating surface. The frequency $f = 0.1$ is therefore the highest frequency at which we can simulate, as the solvent flow will already be zero above the polymer layer at higher frequencies. Even for $f = 0.1$ one might be able to explain the high value of H_{rms} by the fact that the solvent flow hardly penetrates into the polymer layer. To increase the flow within the polymer layer, we increased the amplitude of shear oscillation (to $V_{max} = 80$) and simultaneously brought the upper surface closer to the brush (by setting $L_z = 10$). In this case the polymer density profile still remained virtually indistinguishable from the equilibrium profile.

3.2.4. Results for Parameter Set 2. The values in parameter set 2 ($\rho = 3$ and $a = 25$) are typical ones for DPD simulations of (aqueous) polymer and surfactant solutions.[34,39] The scaling laws for both static and dynamic properties of DPD polymers have been derived using these parameters.[38] The lower overall number density enables us to simulate a larger system for the same CPU time. We consider chains of length $M = 60$, end-tethered to a surface area $L_x \times L_y = 8 \times 8$, with $N_p = 25$.

Under constant shear the response of the polymer brush is very similar to what we observed for parameter set 1. We subjected the brush to shear rates corresponding to Weissenberg numbers *Wi* in the range 0−200. The layer thickness decreased monotonically with increasing shear rate. The response of this brush to oscillatory shear is shown in Figure 13 for reduced oscillation frequencies (τf) in the range 0−2.5. For $f = 0.001$ the brush is compressed with respect to its equilibrium conformation. When the oscillation frequency is increased 1 order of magnitude, a slight further decrease of the layer is observed (this is not shown in the figure). A further increase of the oscillation frequency causes the layer to expand again. For $f = 0.025$ the root-mean-square layer thickness is approximately the same as that of an unsheared brush. At even higher frequencies, H_{rms} increases beyond its equilibrium value. As can be seen from the polymer density profile for $f = 0.05$ in Figure 13, this large value of H_{rms} is primarily due to the appearance of a bulge in the density profile near the upper surface. The reason that the polymer density profile has this nonmonotonic shape at high frequencies is not self-evident.

To explain these observations, we have plotted the total density of the system, solvent plus polymer segments, in Figure 13 for $f = 0.05$. For a steady shear the total density remains nearly constant throughout the system (this is not shown in a figure). In that case, we only observe a deviation from the uniform density very close to the wall. Such a depletion of approximately one molecular layer is normally observed for inhomogeneous systems. In our simulations we further observed that for low-frequency oscillatory shear the total system density remains uniform. However, as can be seen in Figure 13, at high frequencies the total density profile is not uniform at all. Above a critical frequency, we observe a long-range depletion. This depletion extends over 10−15 molecular diameters. Apparently, the oscillating wall causes a long-range repulsive interaction on the fluid particles. The figure also suggests that the polymer segments, because of their macromolecular nature, are less repelled by these effective interactions and expand into the space left by the solvent molecules.

To investigate whether these long-range depletion interactions are specific to polymer brushes, we compared the density profile of a pure solvent in a steady shear field with the same profile in an oscillating shear field. For a pure fluid we observed similar long-range interactions at high oscillation frequencies. These results indicate that the unexpected swelling of the polymer brush at high oscillation frequencies are caused by the properties of the solvent rather than those of the polymer itself. Of course, it remains debatable to what extent these results reflect the behavior of a real molecular system at high (but still experimentally accessible) frequencies and to what extent they are merely an artifact of the coarse-grained DPD model. If the DPD model with this parameter set is realistic, the simulations imply that the threshold frequency needed to induce swelling of the polymer brush is not related directly to the hydrodynamic relaxation time of a blob of the unperturbed brush, as was suggested on theoretical grounds.[19] This hypothesis can, in principle, be tested experimentally.

3.2.5. Discussion. All our simulations indicate that a constant shear flow compresses an end-tethered polymer layer. Although we focused on parameter set 1 to study the effect of constant shear, the results are qualitatively very similar for both parameter sets. For a given shear rate the compression of a grafted polymer layer becomes larger as its grafting density decreases. The smaller layer thickness due to shear is in agreement with previous simulations which treated the solvent flow at the mean-field level (using the Brinkman equation).[22−24] It contradicts a number of theoretical predictions of brush swelling in a solvent flow field.[17−20] In our simulations we considered polymer layers attached to a surface which is at rest. This system is sheared by moving a bare upper surface. In experimental setups one often has a symmetric system with both surfaces covered by polymer. The results which we reported in Figure 5 indicate that moving the lower polymer-bearing surface has exactly the same effect as moving

the upper bare surface. From this one can conclude that our simulations should also give a relevant description of systems where both surfaces are covered with polymer. (Of course, new effects will occur when the polymer layers overlap. This situation has not been investigated in the present paper.)

When exposed to oscillatory shear flow at a not too high frequency, the polymer brush also shows an overall compression, but its structure is continuously adapting to the change in shear flow that it is experiencing. From Figures 11 and 12 for $f = 10^{-4}-10^{-3}$ the picture emerges of a system that can more or less continuously relax in response to the changing shear rate. At a higher frequency ($f = 0.1$) the response of the brush to the oscillating shear becomes much smaller. To a large extent this is due to the lower absolute values of the shear rate at higher frequency, which is an artifact of the simulation model with the present parameter set. The decay length of the solvent velocity profile near an oscillating surface is $(\nu/\pi f)^{1/2}$, where ν is the kinematic viscosity and f the frequency. For water or most common organic liquids this decay length is of the order of 10 μm. In our simulations it is of order $10r_c$ for $f = 0.001$ (i.e., in this case the solvent flow has the opportunity to penetrate well into the brush), but for $f = 0.1$ it is 1 order of magnitude smaller. One can only partly compensate for this strong decrease of the solvent flow by increasing the amplitude of the oscillation.

Using parameter set 2, we do find an increase of H_{rms} beyond its equilibrium value, whereas we did not succeed in clearly finding this effect for parameter set 1. This increase in the layer thickness is due to a depletion force on the solvent near a surface oscillating at a high frequency. The magnitude of this force depends strongly on the parameters used to describe the fluid. For example, increasing the repulsion parameter a, i.e., decreasing the compressibility, gives a weaker depletion. Increasing the particle number density also gives a weaker depletion. For a fluid with the parameters $\rho = 3$ and $a = 10$ we do find a clear depletion zone, although in this case we did not find an increase of the thickness of the polymer brush when sheared. The effect of high-frequency oscillatory shear on a polymer brush in the DPD model seems to depend rather critically on the precise parameters of both the solvent and the polymer.

The major difficulty with the DPD simulations presented in this study is formed by the different time scales that are involved in the systems under consideration. In principle, the most relevant time scale is that of the polymer chains. As a characteristic time τ, one can then take the relaxation time of a free polymer chain in solution. For parameter set 2 ($\rho = 3$, $a = 25$) the dependence of τ on the chain length has been investigated previously.[38] The shear rates and oscillation frequencies which we used in the simulations were chosen such that the reduced numbers $Wi = \dot{\gamma}\tau$ and τf correspond to reasonable experimental values. However, the response of the fluid to an imposed strain is determined by its (kinematic) viscosity ν. Groot and Warren[34] pointed out that (when using parameters similar to those normally used in DPD simulations) the DPD model gives a far too low Schmidt number (which is the dimensionless number obtained from the ratio of the viscosity and the diffusion coefficient). This is the underlying problem which we encountered in Figure 11, where the low solvent viscosity means that the polymer brush can only be sheared at relatively low Wi values. A similar problem occurs with the high-frequency simulations using parameter set 2. The increase of H_{rms} that we saw for $f = 0.05$ in the previous section occurs for a reduced frequency τf of 2. This is a very reasonable experimental value for the frequency. However, if a mapping is made between the simulation and real time scales based on the solvent only, then the frequency does not compare well with a reasonable experimental value. For example, assuming that a solvent particle represent three water molecules and linking its diffusion coefficient to that of real water, we find extremely high frequencies. It is therefore difficult to state whether the effect seen in the simulation model will occur for any molecular system at a reasonable experimental frequency (in the hertz−kilohertz range). This problem is again caused by the poor quantitative description of the fluid dynamics in our present DPD model.

The most straightforward way to improve on the problems mentioned above is to increase the viscosity of the DPD fluid. This can be achieved by increasing both the noise amplitude σ and friction coefficient γ. The increase in the dissipation will then lead to an increased viscosity. As this will not affect the equilibrium properties of the system, it will still be possible to use parameters based on mapping procedures for those properties. However, on the computational side, there will be a penalty associated with a smaller time step. Alternatively, it is also possible to keep the noise amplitude constant but decrease the simulation temperature. However, this will affect the equilibrium properties of the systems that are simulated.

4. Conclusions

The DPD shear simulation approach used in this paper is based on the boundary conditions introduced by Willemsen et al.[45] We have shown that this method is well-suited to model oscillatory shear flow in addition to constant shear flow. Because of its particle-based nature, the DPD method is far better suited for simulations of complex fluids than, for example, computational fluid dynamics methods. As a relevant example of such systems, we have studied the behavior of grafted polymer layers in a shear flow. The (steady-state) problem of a polymer brush under constant shear can be well described with the DPD model. The overall picture that emerges from these simulations is that individual chains become stretched in the direction of flow and that the layer thickness decreases. This agrees fairly well other simulation studies that have been published. However, as solvent particles and hydrodynamic interactions are explicitly taken into account, a full description of the solvent flow within (the tip of) the grafted polymer layer is also acquired from the simulations. Under oscillatory shear, the response of a polymer brush is qualitatively similar to that under constant shear for low oscillation frequencies. In this case the polymer chains are able to follow the continuous change in the flow velocity. At higher frequencies the discrepancy between the time scales of the polymer and solvent dynamics in our DPD model make it difficult to draw definite conclusions regarding the behavior of the systems. Further work is first of all needed here to get a better comprehensive mapping of dynamical properties of a polymer chain and solvent onto the DPD model.

Acknowledgment. We thank Drs. E. Eiser, D. Frenkel, H. Hoefsloot, and C. P. Lowe for stimulating discussions. These investigations are supported in part by the Netherlands Research Council for Chemical Sciences (CW) with financial aid from the Netherlands Technology Foundation and by the Netherlands Organization for Scientific Research (NWO) through PIONIER and Unilever Research Plc.

References and Notes

(1) de Gennes, P. G. *J. Phys.* (*Paris*) **1976**, *37*, 1443.
(2) Alexander, S. J. *J. Phys.* (*Paris*) **1977**, *38*, 983.
(3) Milner, S. T.; Witten, T. A.; Cates, M. E. *Macromolecules* **1988**, *21*, 2610.
(4) Zhulina, E. B.; Borisov, O. V.; Priamitsyn, V. A. *J. Colloid Interface Sci.* **1990**, *137*, 495.
(5) Chakrabarti, A.; Toral, R. *Macromolecules* **1990**, *23*, 2016.
(6) Milner, S. T. *Science* **1991**, *251*, 905.
(7) Auroy, P.; Auvray, L.; Leger, L. *Phys. Rev. Lett.* **1991**, *66*, 719.
(8) Wijmans, C. M.; Scheutjens, J. M. H. M.; Zhulina, E. B. *Macromolecules* **1992**, *25*, 2567.
(9) Grest, G. S.; Murat, M. In *Monte Carlo and Molecular Dynamics Simulations in Polymer Science*; Binder, K.; Ed.; Oxford University Press: New York, 1999; p 476.
(10) Szleifer, I.; Carignano, M. A. In *Advances in Chemical Physics*; Prigogine, I., Rice, S. A., Eds.; Wiley: New York, 1996; Vol. 94, p 165.
(11) Grest, G. S. *Adv. Polym. Sci.* **1999**, *138*, 149.
(12) Klein, J.; Perahia, D.; Warbourg, S. *Nature (London)* **1991**, *352*, 143.
(13) Nguyen, D.; Clarke, C. J.; Eisenberg, A.; Rafailovich, M. H.; Sokolov, J.; Smith, G. S. *J. Appl. Crystallogr.* **1997**, *30*, 680.
(14) Baker, S. M.; Smith, G. S.; Anastassopoulos, D. L.; Toprakcioglu, C.; Vradis, A. A.; Bucknall, D. G. *Macromolecules* **2000**, *33*, 1120.
(15) Ivkov, R.; Butler, P. D.; Satija, S. K.; Fetters, L. J. *Langmuir* **2001**, *17*, 2999.
(16) Rabin, Y.; Alexander, S. *Europhys. Lett.* **1990**, *13*, 49.
(17) Barrat, J. L. *Macromolecules* **1992**, *25*, 832.
(18) Kumaran, V. *Macromolecules* **1993**, *26*, 2464.
(19) Harden, J. L.; Cates, M. E. *Phys. Rev. E* **1996**, *53*, 3782.
(20) Aubuoy, M.; Harden, J. L.; Cates, M. E. *J. Phys. II* **1996**, *6*, 969.
(21) Clement, F.; Charitat, T.; Johner, A.; Joanny, J.-F. *Europhys. Lett.* **2001**, *54*, 65.
(22) Parnas, R. S.; Cohen, Y. *Rheol. Acta* **1993**, *33*, 485.
(23) Doyle, P. S.; Shaqfeh. E. S. G.; Gast, A. P. *Phys. Rev. Lett.* **1997**, *78*, 1182; *Macromolecules* **1998**, *31*, 5474.
(24) Saphiannikova, M. G.; Pryamitsyn, V. A.; Cosgrove, T. *Macromolecules* **1998**, *31*, 6662.
(25) Neelov, I.; Borisov, O. V.; Binder, K. *Macromol. Chem. Theor. Simul.* **1998**, *7*, 141.
(26) Lai, P.-Y.; Binder, K. *J. Chem. Phys.* **1993**, *98*, 2366.
(27) Miao, L.; Guo, H.; Zuckermann, M. J. *Macromolecules* **1996**, *29*, 2289.
(28) Lai, P.-Y.; Lai, C.-Y. *Phys. Rev. E* **1996**, *54* 6958. Lai, C.-Y.; Lai, P.-Y. *Macromol. Theor. Simul.* **1997**, *6*, 835.
(29) Peters, G. H.; Tildesley, D. J. *Phys. Rev. E* **1995**, *52*, 1882; **1996**, *54*, 5493.
(30) Grest, G. S. *Phys. Rev. Lett.* **1996**, *76*, 4979.
(31) Hoogerbrugge, P. J.; Koelman, J. M. V. A. *Europhys. Lett.* **1992**, *19*, 155.
(32) Koelman, J. M. V. A.; Hoogerbrugge, P. J. *Europhys. Lett.* **1993**, *21*, 363.
(33) Kong, Y.; Manke, C. W.; Madden, W. G.; Schlijper, A. G. *Int. J. Thermophys.* **1994**, *15*, 1093.
(34) Groot, R. D.; Warren, P. B. *J. Chem. Phys.* **1997**, *107*, 4423.
(35) Groot, R. D.; Madden, T. J.; Tildesley, D. J. *J. Chem. Phys.* **1999**, *110*, 9739.
(36) Venturoli, M.; Smit, B. *Phys. Chem. Commun.* **1999**, *10*.
(37) Jury, S.; Bladon, M.; Cates, M.; Krishna, S.; Hagen, M.; Ruddock, N.; Warren, P. *Phys. Chem. Chem. Phys.* **1999**, *1*, 2051.
(38) Spenley, N. A. *Europhys. Lett.* **2000**, *49*, 534.
(39) Groot, R. D. *Langmuir* **2000**, *16*, 7493.
(40) Malfreyt, P.; Tildesley, D. J. *Langmuir* **2000**, *16*, 4732.
(41) Español, P.; Warren, P. B. *Europhys. Lett.* **1995**, *30*, 191.
(42) Allen, M. P.; Tildesley, D. J. *Computer Simulations of Liquids and Solids*; Clarendon Press: Oxford, 1987.
(43) Jones, J.; Lal, M.; Ruddock, J. N.; Spenley, N. A. *Faraday Discuss.* **1999**, *112*, 129.
(44) Revenga, M.; Zúñiga, I.; Español, P.; Pagonabarraga, I. *Int. J. Mod. Phys. C* **1998**, *9*, 1319.
(45) Willemsen, S. M.; Hoefsloot, H. J. C.; Iedema, P. D. *Int. J. Mod. Phys. C* **2000**, *11*, 881.
(46) Wijmans, C. M., unpublished results.
(47) Churchill, S. W. *Viscous Flows*: *The Practical Use of Theories*; Butterworth: Boston, 1988.
(48) Marsh, C. A.; Backx, G.; Ernst, M. H. *Phys. Rev. E* **1997**, *56*, 1676.
(49) Pagonabarraga, I.; Hagen, M. H. J.; Frenkel, D. *Europhys. Lett.* **1998**, *42*, 277.
(50) Masters, A. J.; Warren, P. B. *Europhys. Lett.* **1999**, *48*, 1.
(51) Carslaw, H. S.; Jaeger, J. C. *Conduction of Heat in Solids*, 2nd ed.; Clarendon Press: Oxford, 1959.
(52) Schlichting, H. *Grenzschicht-Theorie*; Braun: Karlsruhe, 1958.
(53) Wijmans, C. M.; Smit, B.; Groot, R. D. *J. Chem. Phys.* **2001**, *114*, 7644.
(54) The statistical fluctuations in the simulated flow profiles are too large to be able to find d^2v/dz^2 directly by numerical differentation. Instead, we calculated the first derivative dv/dz numerically, then fitted a sigmoidal curve through this first derivative, and differentiated that curve to find the second derivative d^2v/dz^2.

MA020086B